P1.2 ON ROTORS, INTERNAL WAVES AND HYDRAULIC JUMPS IN SIMULATED STABLY-SRATIFIED FLOWS IN UTAH'S SALT LAKE VALLEY

Ying Chen*, R. L. Street, F. L. Ludwig

Stanford University, Stanford, California

1. Introduction

The Advanced Regional Prediction System (ARPS) was used to simulate weak synoptic wind condition with stable stratification and pronounced drainage flow at night in the vicinity of the Jordan Narrows at the south end of the Salt Lake Valley. The simulations showed the flow to be quite complex with hydraulic jumps and internal waves that make it essential to use a complete treatment of the fluid dynamics. Agreement between simulations and observations from the October 2000 Vertical Transport and Mixing eXperiment (VTMX) was qualitatively good, and usually quantitatively good as well. More flow features were resolved at finer spatial resolutions. Five one-way nested grids were used to resolve the complex topography and flow features. A coarse ARPS model grid with horizontal spacing of 20 km was initialized by ETA 40-km operational analyses. Model outputs on that grid were input to finer grids with horizontal resolution of 5 km, 1 km, 250 m and 100 m via one-way nesting. The 250-m and 100-m grids have 200 vertically stretched levels up to a height of 20 km. The vertical spacing is 10 m at the surface, and 190 m at the uppermost level. Figure 1 shows the relationship of the 1-km, 250-m and 100-m Grids.

2. Simulated rotors, internal waves and hydraulic jumps

Figure 2 is a perspective view of the area covered by the 100-m grid. The terrain complexity is substantial, but exaggerated by a 10:1 ratio between vertical and horizontal scales. Simulation results are displayed in Figure 3 to Figure 8 for the three cross sections shown in Figure 2. Flows in the north-south corss sections at the Traverse Range show how stratified nighttime flow interacts with the mountain barrier.

The simulated results from 100-m grid show that the flow over the Traverse Mountain barrier can induce wave motions in the lee, along with low-level rotor flow that is associated with internal waves and hydraulic jumps. Figures 3, 5 and 7 show the evolution of ARPS winds and temperatures in the cross sections A, B and C (see Figure 2). Figures 4, 6 and 8 are the enlarged views of the wind field for Figures 3, 5 and 7 respectively, where some interesing flow features can be seen more clearly.

There is a well established, early evening (0200 UTC or 1900 LST) northerly flow in Figures 3a, 5a and 7a. It comes up the Salt Lake Valley, over the Traverse Moutains and into the Utah Lake basin. The subsidence over the south slope of the Traverse Mountains is quite strong in the lowest kilometer, and a stable shallow layer is produced on the lee slope (Figures 3a, 5a and 7a). Flow decelerates upon encountering flatter terrain, and an hydraulic jump is produced (Figures 4 and 8). As the night progresses and the surface cools, the flow reverse. Winds reversed by 0600 UTC (2300 LST, Figures 3b, 5b and 7b). The winds near the surface were weak at this time, and became stronger at 1000 UTC (0300 LST, Figures 3c, 5c and 7c). Flow separation occurs at the foot of the mountain and rotors are formed (Figure 6).

3. Conclusion

Our results indicate that using ARPS model and nested grid methods has allowed us to produce hydraulic jumps, internal waves and rotors over a complex orography. Those flows can have a large effect on mixing and vertical transport. The simulations may not precisely reproduce the real flows, but they can aid in the design of the future field experiments.

Acknowledgments: The work was supported by the Atmospheric Sciences Program, Office of Biological and Environmental Research, U.S. Department of Energy. The National Energy Research Scientific Computing Center provided computational time. We gratefully acknowledge Professor Ming Xue and others at the University of Oklahoma for their help.

*Corresponding author address: Ying Chen, Stanford Univ., Environmental Fluid Mechanics Lab., Civil and Environmental Engineering, Stanford CA 94061-4020; email: yingchen@stanford.edu

References

[1] Chen, Y., F. L. Ludwig, and R. L. Street, 2004: Stably-stratified flows near a notched, transverse ridge across the Salt Lake Valley. *J. Appl. Meteor.*, in press.

[2] Doran, J. C., J. D. Fast, and J. Horel, 2002: The VTMX 2000 campaign. *Bulletin of American Meteorological Society*, **83**(4), 537-551.

[3] Ludwig, F. L., J. Horel, and C. D. Whiteman, 2004: Using EOF analysis to identify important surface wind patterns in mountain valleys. *J. Appl. Meteor.*, in press.

[4] Xue, M., K. K. Droegemeier, V. Wong, A. Shapiro, and K. Brewster, 1995: *ARPS Version 4.0 User's Guide*, Center for Analysis and Prediction of Storms, University of Oklahoma, 380 pp.

[5] Xue, M., K. K. Droegemeier, and V. Wong, 2000. The Advanced Regional Prediction System (ARPS) - A multiscale nonhydrostatic atmospheric simulation and prediction tool. Part I: Model dynamics and verification. *Meteor. Atmos. Phys.*, **75**, 161-193.

[6] Xue, M., K. K. Droegemeier, V. Wong, A. Shapiro, K. Brewster, F. Carr, D. Weber, Y. Liu, and D. H. Wang, 2001. The Advanced Regional Prediction System (ARPS) - A multiscale nonhydrostatic atmospheric simulation and prediction tool. Part II: Model physics and applications. *Meteor. Atmos. Phys.*, **76**, 134-165.

[7] Xue, M., D. H. Wang, J. D. Gao, K. Brewster,and K. K. Droegemeier, 2003. The Advanced Regional Prediction System (ARPS), storm-scale numerical weather prediction and data assimilation, *Meteor. Atmos. Phys.*, **82**,139-170

[8] Zhong, S. and J. D. Fast, 2003: An evaluation of MM5, RAMS, and Meso Eta at sub-kilometer resolution using VTMX field campaign data in the Salt Lake Valley. *Monthly Weather Review*, **131**, 1301-1322.

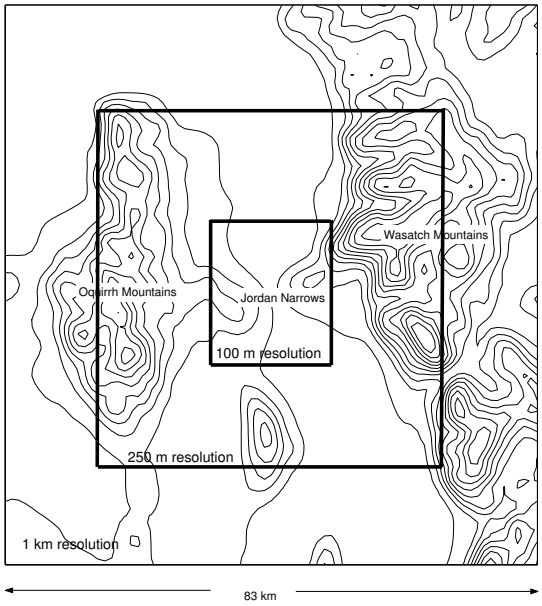

Fig.1. The three computational grids.

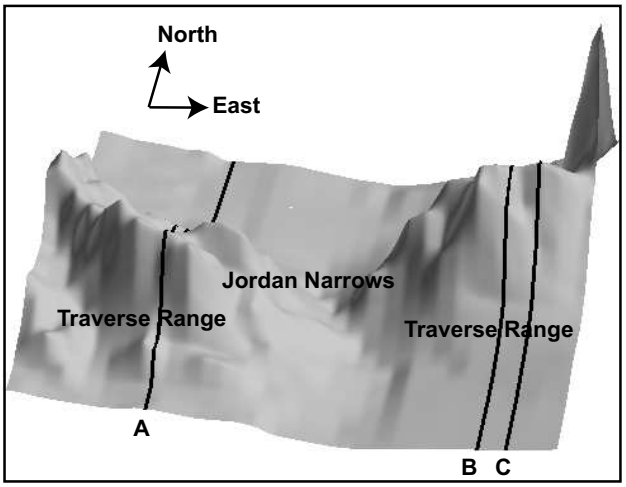

Fig.2. Perspective view of the terrain encompassed by the 100-m grid.

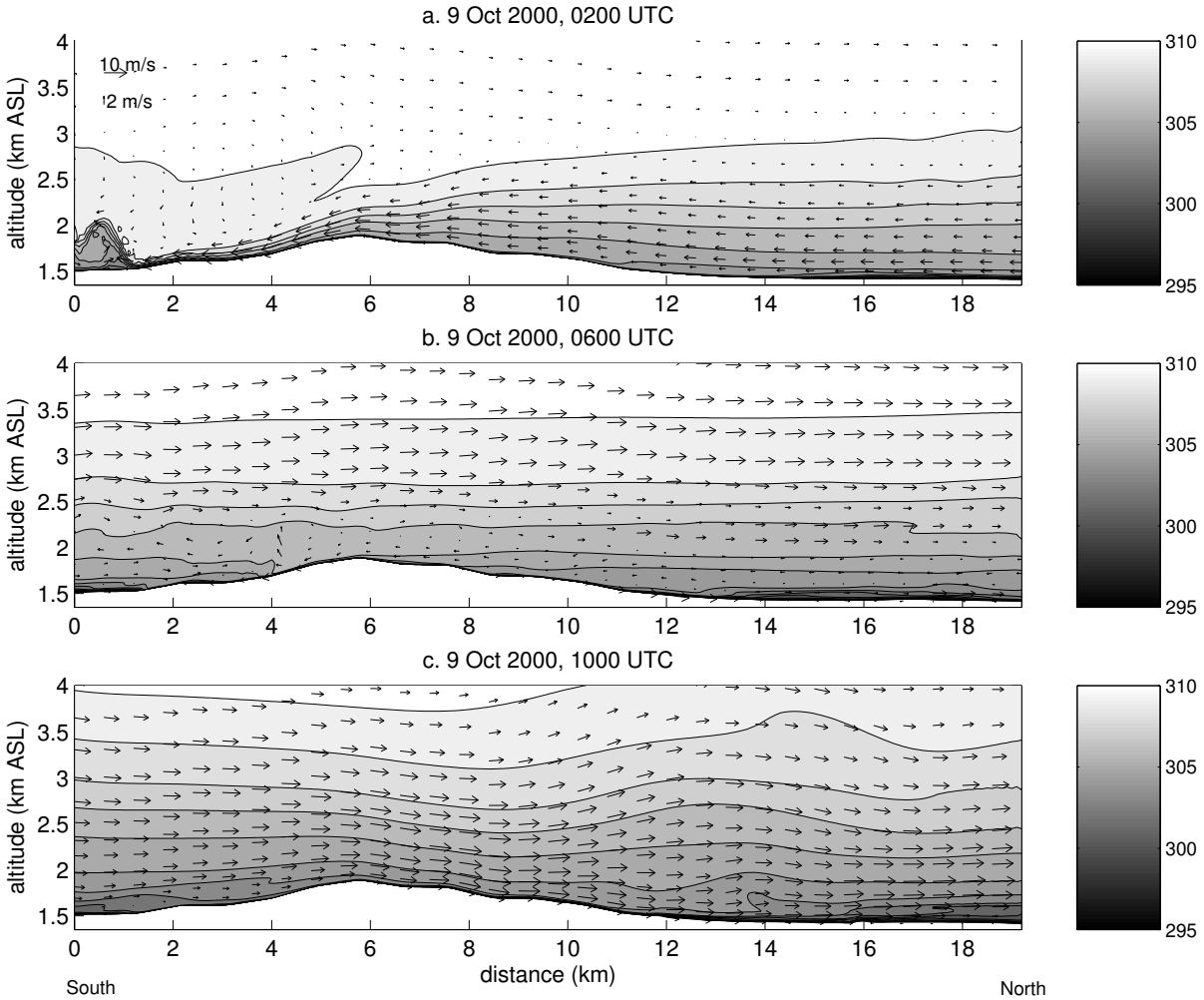

Fig.3. Evolution of ARPS winds and temperatures in the cross section A (see Figure 2).

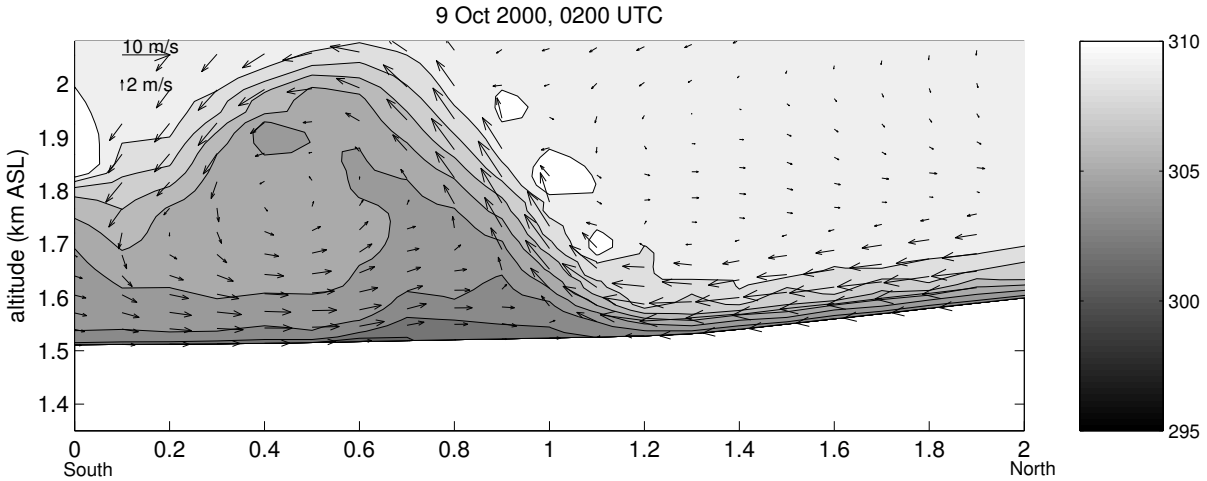

Fig.4. The enlarged view of a part of Figure 3a.

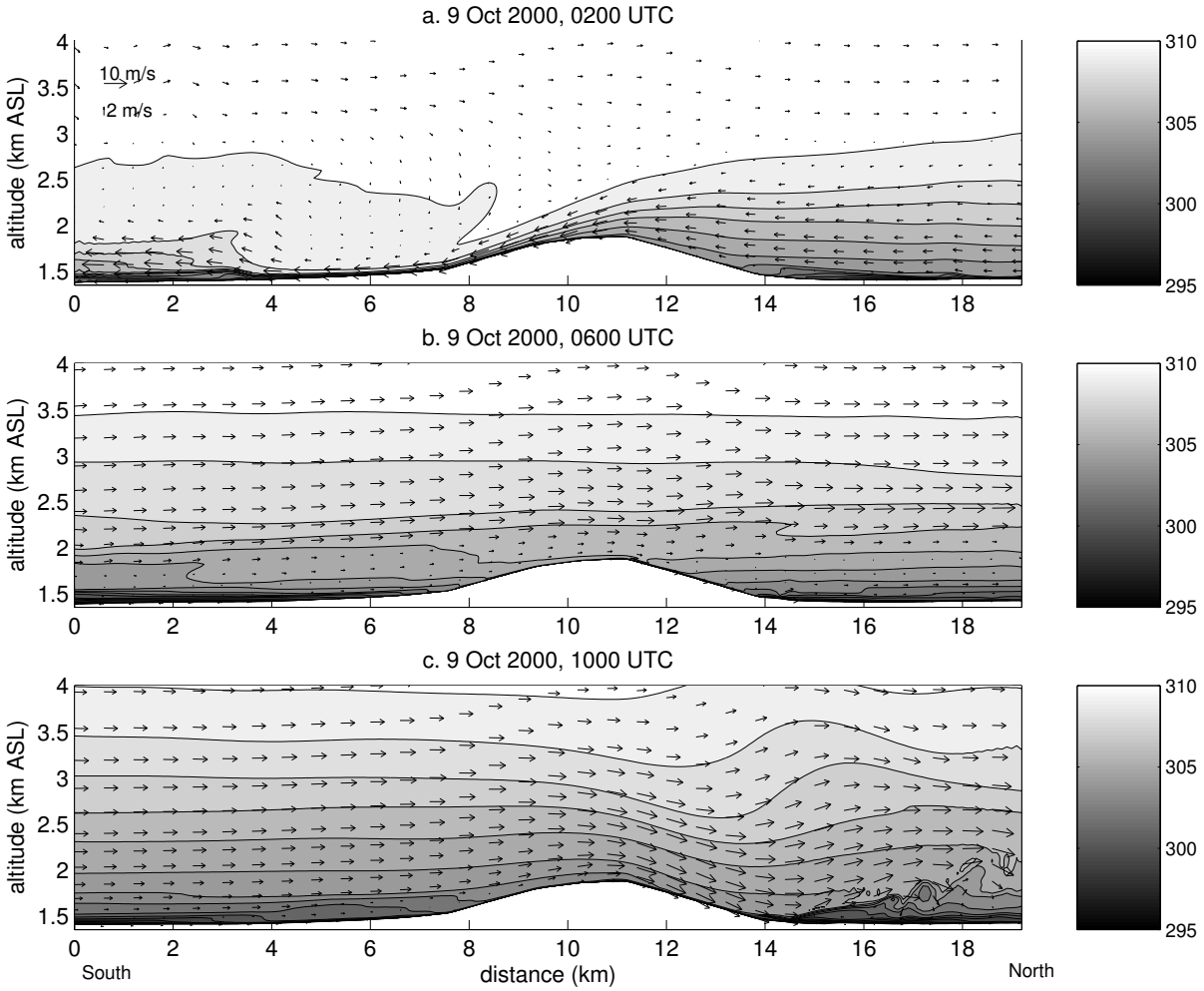

Fig.5. Evolution of ARPS winds and temperatures in the cross section B (see Figure 2)

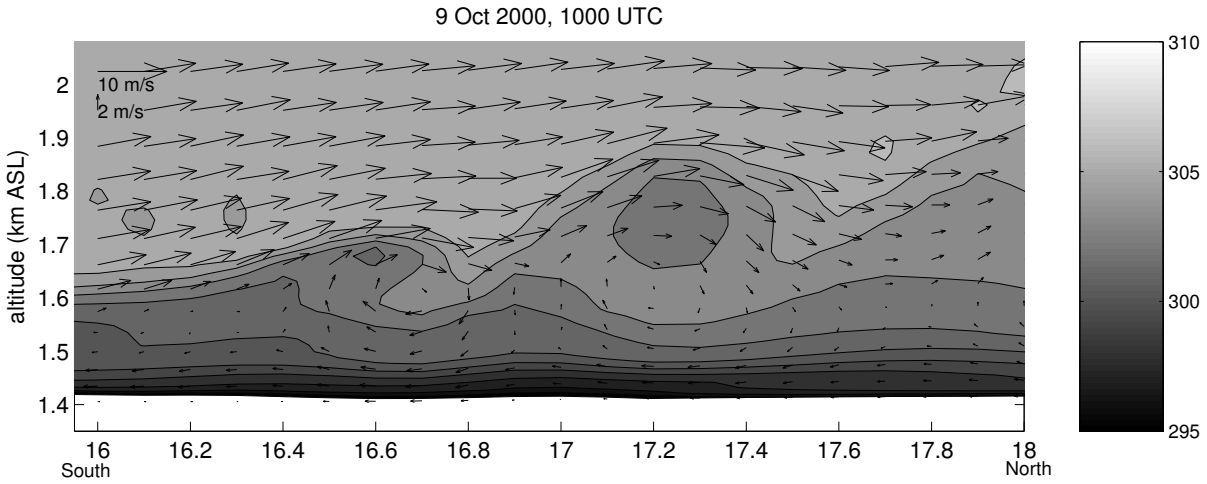

Fig.6. The enlarged view of a part of Figure 5c.

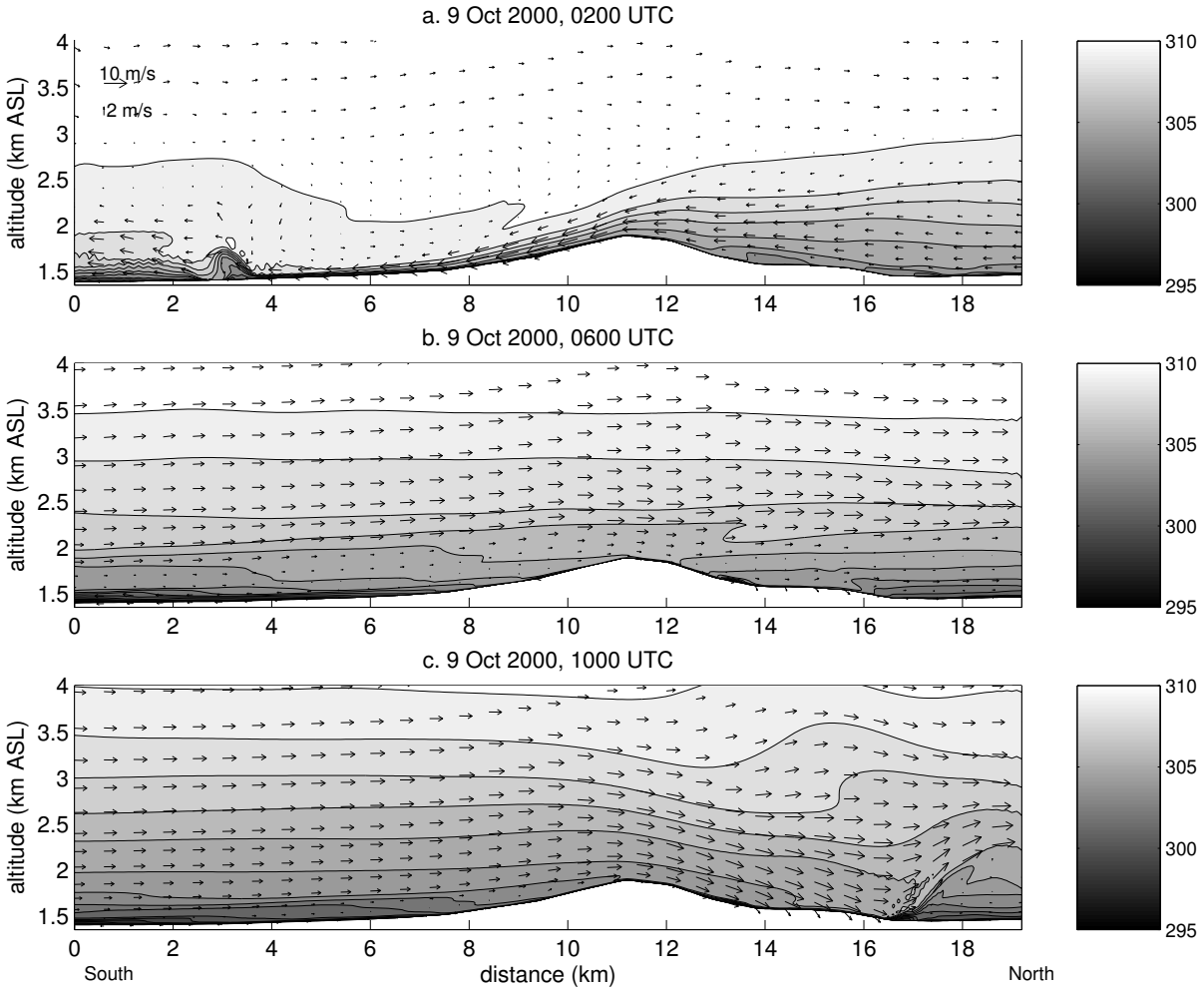

Fig.7. Evolution of ARPS winds and temperatures in the cross section C (see Figure 2)

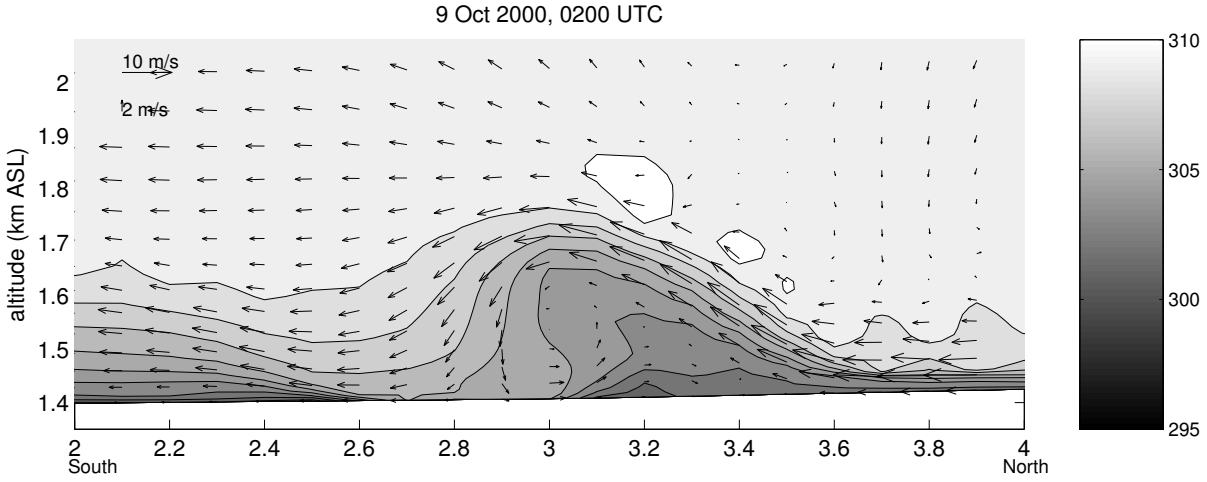

Fig.8. The enlarged view of a part of Figure 7a.